



Seasonal and Spatial Variations of Chemical Weathering in the Mekong Basin: From the Headwaters to the Lower Reaches

Hiroto Kajita^{1,2,3,4} · Yuki Ota³ · Toshihiro Yoshimura⁴ · Daisuke Araoka³ · Takuya Manaka⁵ · Ouyang Ziyu² · Shinya Iwasaki⁴ · Takuya Yanase^{1,2} · Akihiko Inamura³ · Etsuo Uchida⁶ · Hongbo Zheng⁷ · Qing Yang⁷ · Ke Wang^{2,7} · Atsushi Suzuki³ · Hodaka Kawahata^{1,2,3}

Received: 27 December 2019 / Accepted: 8 April 2020 / Published online: 23 April 2020
© Springer Nature B.V. 2020

Abstract

Chemical weathering in the Himalayan river basins is among the highest in the world and has received vast research attention related to past climate change. Many early estimates of chemical weathering are based on a small number of water property data that ignore those spatial and seasonal variations. Therefore, this study analyzed spatial and seasonal variations in chemical weathering in the Mekong Basin, where the geology, climate, and hydrologic cycle of the basin vary significantly from the lower to upper reaches and from dry to rainy seasons. We separately estimated the origins of dissolved elements and potential CO₂ consumption rates using the numerous chemical compositions of river water throughout the entire basin and in both seasons. The CO₂ consumption rate in the rainy season is three to five times that in the dry season that may be due to the high temperature and precipitation. Despite the low temperatures and dryness of the upper and middle basins, the CO₂ consumption rate is approximately twice that in the lower reaches; this can be attributed to active physical denudation in steep mountainous areas which increases the surface area for water–rock interactions. The total CO₂ consumption obtained by combining each season and basin was $48\text{--}70 \times 10^9$ mol/a and $148\text{--}159 \times 10^9$ mol/a for silicate and carbonate weathering, respectively, which are almost half the values of previous estimates. Our results suggest that seasonally and spatially separated evaluations are important for generating estimates of chemical weathering in large Himalayan rivers.

Keywords Mekong river · Chemical weathering · Carbon cycle · Seasonal variation · Spatial variation

Electronic supplementary material The online version of this article (<https://doi.org/10.1007/s10498-020-09374-y>) contains supplementary material, which is available to authorized users.

✉ Hiroto Kajita
kajita322@frontier.hokudai.ac.jp

Extended author information available on the last page of the article

1 Introduction

Chemical weathering is a key earth-surface process that links element cycling of the solid Earth to the atmosphere and oceans (Berner 2003). Terrestrial weathering forms a major atmospheric CO₂ sink that generates bicarbonate as dissolved inorganic carbon (DIC). The DIC is transported to the ocean by rivers and released to the atmosphere in the form of CO₂ through oceanic carbonate mineralization processes. The difference in the molar ratio of CO₂ consumed by silicate and carbonate weathering during this process suggests that only silicate weathering is a net atmospheric CO₂ sink (Berner et al. 1983; Berner 2003). Therefore, evaluating weathering fluxes and clarifying their controlling factors are very important for understanding the roles of rivers in the global carbon cycle and climate change on a geological timescale (Amiotte Suchet et al. 2003). However, it is difficult to determine the sensitivity of continental chemical weathering to climatic parameters (temperature and precipitation) and other potential controls such as physical denudation and vegetation (White and Blum 1995).

The Himalayas are the highest and steepest mountains in the world. Active physical denudation caused by ongoing uplift of the Himalayan–Tibetan Plateau and heavy rains associated with the Asian and Indian Monsoons increase chemical weathering rates in this region (Yin and Harrison 2000; Hodges 2006). Gaillardet et al. (1999) compiled data on large rivers in the world and estimated that approximately 20% of total global CO₂ consumption occurs in the Himalayan river basins. According to the hypothesis of Raymo and Ruddiman (1992), the global cooling trend is observed since the Eocene may have been triggered primarily by high chemical weathering rates as a result of the newly uplifted Himalayan orogeny. Therefore, studying the chemical weathering rates in the Himalayas and their controlling factors is essential considering their crucial role in global carbon cycles and climate change.

Previous studies have used modeling approaches based on the chemical components of river water to estimate the total amount of chemical weathering in river basins and the relative contributions of different rocks (e.g., Galy and France-Lanord 1999). However, some early studies used only a small number of chemical property data observed in the lower reaches or only quoted from local government or private organization reports (Meybeck and Ragu 1997). Therefore, it is important to reevaluate the chemical compositions of these rivers to ensure accurate assumptions of total CO₂ consumption (e.g., Manaka et al. 2015a). Seasonal and spatial variations of the chemical components should be also carefully considered when evaluating total CO₂ consumption in the Himalayan river basins because the lithology and climate vary considerably from the upper to lower reaches and temperature, precipitation, and physical denudation have substantial effects on weathering intensity (Tipper et al. 2006; Rai and Singh 2007; Singh et al. 2008; Manaka et al. 2017; Zhong et al. 2017). Quantifying chemical weathering in each sub-basin and season is important not only for obtaining more plausible calculations of total CO₂ consumption, but also for clarifying the effects of controlling factors, such as climate, topography, geology, and human activities, on chemical weathering intensity (Wang et al. 2016; Bastia and Equeenuddin 2019; Samanta et al. 2019; Yu et al. 2019).

The Mekong River is one of the largest rivers in the Himalayas. It is the eighth largest river in the world in terms of water discharge (approximately 467 km³/a) and the twelfth largest in terms of length (approximately 4650 km) (Meybeck and Ragu 2012). It transports 467 km³/a and 1.5×10^{14} g/a of water and sediment to the South China Sea, respectively (Meybeck and Ragu 2012). It is characterized by some of the most complex

hydrologic, climatic, and physiographic features in the world; it originates from the arid Tibetan Plateau, then flows down the steep and geologically complex valleys to Southeast Asia under the influence of the monsoon. Despite its significance, the spatial variations of major element characteristics and related controlling mechanisms of the Mekong River have not been well studied, especially in the upper reaches. The water characteristics in the upper reaches have previously been reported by Wu et al. (2008a) and Noh et al. (2009); however, the number of data is particularly small in the dry season. For the lower reaches, Li et al. (2014) calculated the amount of chemical weathering based on internal data provided by the Mekong River Commission (MRC) for the twentieth century. In this study, we provide a new dataset of the chemical composition of the Mekong River from the lower to upper reaches in both the dry and rainy seasons. This research will contribute to our understanding of chemical weathering and element cycles not only in the Mekong Basin, but also in the other Himalayan rivers.

2 Methods

2.1 Study Area

The Mekong River originates in the eastern part of the Tibetan Plateau and flows through China, Myanmar, Laos, Thailand, Cambodia, and Vietnam, draining a 795000 km² watershed to the ocean (MRC 2005). In this study, we divided the Mekong Basin into three general sub-basins, the upper Mekong Basin (UMB) in China (above Gajiu; 114500 km²), the middle Mekong Basin (MMB) (from Gajiu to Chiang Sean; 80500 km²), and the lower Mekong Basin (LMB) (below Chiang Sean; 600000 km²) (Fig. 1). From its headwaters in the high mountains running from north to south (~4500 m elevation), the river flows through relatively steep and narrow gorges in the UMB, with the rate of descent becoming more gradual as it approaches the South China Sea (Fig. 1).

Precipitation and air temperature data were collected in several cities in the Mekong Basin (Fig. S1). These data were provided by the Japan Meteorological Agency, which compiles data from meteorological stations in each country. The climate is strongly influenced by the Asian and Indian Monsoons, which brings heavy summer rainfall. In the LMB and MMB, mean annual precipitation is 1370 mm and 1448 mm, respectively, more than 80% of which falls from May to December. In this study, we defined December to May and June to November as the dry and rainy seasons, respectively. The UMB is arid, especially in winter, and the mean annual precipitation is 450 mm. The mean annual air temperature of the Mekong Basin increases downstream, from 8 °C in the UMB to 28 °C in the LMB. Daily water level and discharge data of the Mekong River are monitored by the MRC in several cities in Laos, Thailand, Cambodia, and Vietnam. The water level in the rainy season fluctuates by up to 10 times more than that in the dry season. As the highest water level is observed in August or September, we subdivided the rainy season into the flooding season and subsiding season, as shown in Fig. 2b.

A lithological map of the Mekong Basin was obtained from the Coordinating Committee for Geoscience Programmes in East and Southeast Asia (CCOP) (Fig. S3). The Mekong River flows over a major Paleozoic–Mesozoic sedimentary sequence intercalated with evaporite rock in the UMB, which predominantly comprises folded sedimentary and Precambrian metamorphic rocks (sandstone, shale, schist, chert, and limestone). In the eastern margin of the Tibetan Plateau, called the “Three Rivers area,” where three large rivers

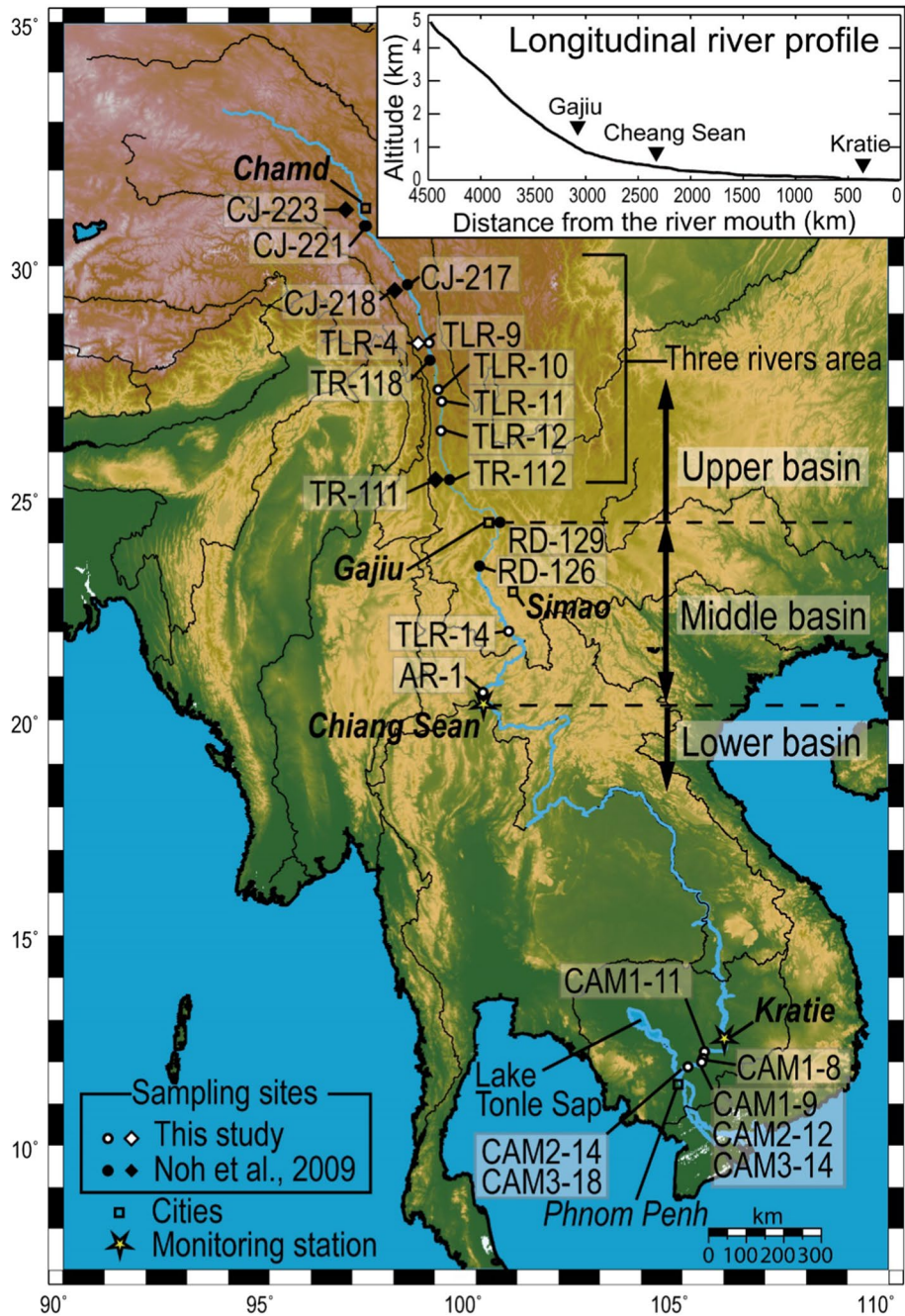


Fig. 1 Locations of study sites and monitoring stations on the Mekong River. Water sampling locations in the mainstream and the headwaters of small tributaries are represented by circles and rhombuses, respectively. Inset shows the longitudinal profile of the Mekong River based on MRC (2005)

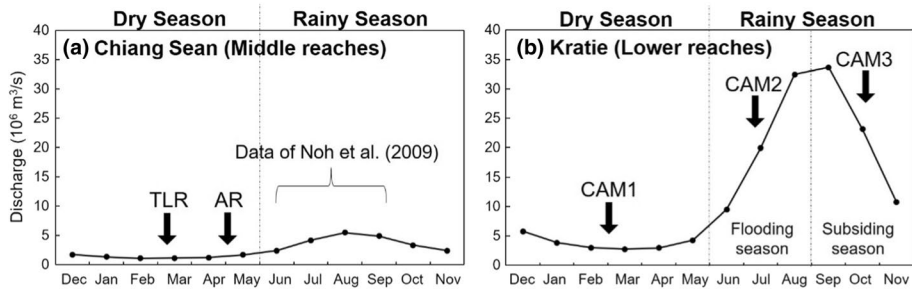


Fig. 2 Average monthly water discharge of the Mekong River from 2000–2016 observed at: **a** Chiang Sean monitoring station, and **b** Kratie monitoring station. Data were obtained from the MRC. Arrows indicate the times of each survey

(upper Mekong, Yangtze, and Salween Rivers) flow parallel within a range of only 100 km forming valleys up to 3000 m deep, the lithology is particularly complicated and includes volcanic rocks and plutonic felsic rocks, which were formed by collision of the Indian and Eurasian plates (Wang and Burchfiel 2000; Feng 2002). The surface lithology of the MMB is mainly Jurassic to Cretaceous carbonate consolidated sedimentary rocks and Carboniferous to Permian limestones (Xiaochi et al. 2003). The Precambrian basement with medium–highly metamorphic and predominantly granitic characteristics is also exposed around this area. The river flows through a strip of Quaternary alluvium in the northern part of the LMB then over Mesozoic sedimentary and metamorphic rocks (mainly sandstone and mudstone) until it reaches northern Cambodia where alluvium with outcrops of Triassic sedimentary rocks and Neogene basalts is exposed (Gupta et al. 2009). The lithological compositions are as follows: 8.4% for sands and sandstones, 43.2% shales, 21.4% carbonate rocks, 18.2% shield rocks, 2.9% acid volcanic rocks, and 5.8% basalts (Amiotte Suchet et al. 2003).

2.2 Sampling Protocols

To evaluate the spatial and seasonal variations in the chemical composition of the Mekong River, we conducted field surveys to collect samples from the headwaters of small tributaries in the Three Rivers area and the mainstream of the Mekong River (Figs. 1, S2). In the dry season, we collected six samples from the UMB and MMB (TLR survey; February 22–March 7, 2019), one sample from the Myanmar–Laos border (AR survey; May 7, 2016), and three samples from the LMB (CAM1 survey; February 23–24, 2016). In the rainy season, we sampled the LMB during both the flooding season (CAM2 survey; July 9–10, 2016) and subsiding season (CAM3 survey; October 12–14, 2016) because the amount of water differs significantly in the two seasons. In the LMB, we collected water samples upstream of the confluence of the Tonle Sap River to avoid the influence of the reverse flow from Lake Tonle Sap. These sampling points are not affected by seawater intrusion, as often observed in the Mekong delta in Vietnam (e.g., Tran et al. 2019). For data from the UMB during the rainy season, we cited those of Noh et al. (2009), who collected water samples from June to September. The sampling sites (in the format sampling survey—sampling number) and the timing of each sampling survey (TLR, AR, CAM1, CAM2, CAM3) are shown in Figs. 1 and 2, respectively.

Water temperature and pH were measured in situ, simultaneous to water sample collections for laboratory analysis. We used two portable pH meters (model 826 Mobile, Metrohm, and LAQUA twin pH-33B, Horiba) for pH measurements. Values were measured with an accuracy of ± 0.05 for each piece of equipment. Samples for laboratory analysis were filtered through acetate membrane filters (pore size: 0.45 μm). Subsamples for each measurement procedure were stored separately in glass vials or polypropylene bottles. Samples for total alkalinity were immediately dosed with HgCl_2 to prevent further biological activity.

2.3 Laboratory Analysis

Cation (Na, K, Ca, and Mg) concentrations were measured by inductively coupled plasma-atomic emission spectrometry (iCAP-6300, Thermo Scientific) at National Institute of Advanced Industrial Science and Technology, Japan (AIST). Anion concentrations (Cl , NO_3 , and SO_4) were measured at AIST and Japan Agency for Marine-Earth Science and Technology (JAMSTEC) using an ion chromatograph (930 Compact IC Flex, Metrohm AG and ICS-2100, Thermo Fisher Scientific Inc.). The analytical error for the ion concentrations was $\pm 3\%$ (2 relative standard deviations) as estimated from the reproductivity of standard solutions. We measured the total alkalinities with an automated titrimetric analyzer (Radiometer, ABU91) through potentiometric titration at 25 °C. The two standard deviations of the measurements were within 10 $\mu\text{mol/kg}$. We calculated the HCO_3 and DIC concentrations from the in situ temperature, pH, and total alkalinity values using the carbonate equilibrium calculation program CO2calc (Robbins et al. 2010) based on the equilibrium constants (K_1 and K_2) proposed by Millero (1979).

3 Results

3.1 pH, DIC, and Total Alkalinity

The pH was mildly alkaline for all analyzed samples, with mean values of 8.4 and 7.7 in dry and rainy seasons, respectively. High pH values were measured in the UMB and MMB and low values were measured in the LMB, especially in the rainy season. Total alkalinity and DIC values in the dry season were 1168–2922 $\mu\text{Eq/L}$ and 1169–2892 $\mu\text{mol/L}$, which were higher than those during the rainy season (512–2444 $\mu\text{Eq/L}$) and 518–2471 $\mu\text{mol/L}$, respectively. Total alkalinity and DIC values were relatively low in the headwaters and significantly higher in the mainstream of the Three Rivers area; the values then decreased downstream. Notably low values were recorded in the lower reaches in the rainy season. All pH, DIC, and total alkalinity data are listed in Table 1.

3.2 Dissolved Major Ions

Major element concentrations are listed in Table 1. The trilinear diagram of the major ion composition shows that the chemical properties of samples collected from surveys in different years could be grouped by the unique chemical characteristics of each sampling location (headwaters, UMB, MMB, and LMB) in the two different seasons (Fig. 3). Therefore, we believe that our compiled data represent typical values of the Mekong River water

Table 1 Sample information and dissolved major element concentrations

Location	Data source	Sample name	Latitude (°N)	Longitude (°E)	Date	temp (°C)	pH	Na (μmol/L)	K	Ca	Mg	Cl	SO ₄	NO ₃	HCO ₃	
<i>Dry season</i>																
Headwater	This study	TLR-04	28.40	98.78	2019/2/22	6.1	8.49	37	33	646	117	3.62	179	13.5	1146	
UMB	This study	TLR-09	28.37	98.86	2019/2/23	6.2	8.74	1223	55	1686	866	936	1140	37.3	2831	
UMB	This study	TLR-10	27.36	99.09	2019/2/24	6.7	8.29	1062	51	1588	811	834	1038	36.4	2754	
UMB	This study	TLR-11	27.10	99.17	2019/2/24	8.2	8.64	1043	51	1589	801	809	1017	35.8	2678	
UMB	This study	TLR-12	26.47	99.15	2019/2/25	6.2	8.35	976	49	1568	764	770	987	37.4	2705	
MMB	This study	TLR-14	22.01	100.80	2019/3/7	19.2	7.95	369	42	955	431	273	461	37.1	1835	
MMB	This study	AR-1	20.63	100.17	2016/5/7	–	–	361	45	932	394	314	407	30.5	–	
LMB	This study	CAM1-11	12.25	105.53	2016/2/24	29.1	8.43	337	45	640	279	246	208	14.3	1594	
LMB	This study	CAM1-8	12.07	105.50	2016/2/23	28.0	8.20	336	46	642	283	259	209	14.1	1562	
LMB	This study	CAM1-9	11.99	105.47	2016/2/23	28.3	8.51	334	46	632	285	262	199	14.7	1546	
<i>Rainy season</i>																
Headwater	✳	CJ-218	29.54	98.26	2000/6/6	8.2	7.82	46.2	9.6	283	91.5	10	79.7	–	507	
Headwater	✳	CJ-223	31.28	96.61	2000/6/7	9.4	8.22	72.5	18.1	883	572	13.8	326	–	2176	
Headwater	✳	TR-111	25.48	99.22	2004/8/9	18.2	7.58	95.2	25.4	466	71.8	25.2	84.3	–	1056	
UMB	✳	CJ-221	30.84	97.34	2000/6/7	16.9	7.21	494	33.3	940	420	303	432	–	2035	
UMB	✳	CJ-217	29.61	98.34	2000/6/6	15.6	7.66	697	54.1	1110	484	482	526	–	2167	
UMB	✳	TR-118	28.47	98.82	2004/8/11	19.3	8.14	591	37.5	1070	543	380	584	–	2416	
UMB	✳	TR-112	25.39	99.29	2004/8/9	20.6	7.96	368	25.4	985	430	212	405	–	2494	
MMB	✳	RD-129	24.46	100.44	2001/9/10	23.0	8.44	326	34.1	891	371	164	340	–	1968	
MMB	✳	RD-126	23.56	100.18	2001/9/9	23.5	8.4	278	35.3	796	319	136	298	–	1805	
LMB	This study	CAM2-12	11.99	105.47	2016/7/9	29.3	7.39	385	50	373	158	364	97	40.4	873	

Table 1 (continued)

Location	Data source	Sample name	Latitude (°N)	Longitude (°E)	Date	temp (°C)	pH	Na (µmol/L)	K	Ca	Mg	Cl	SO ₄	NO ₃	HCO ₃
LMB	This study	CAM2-14	11.75	105.00	2016/7/10	29.8	7.49	371	50	360	152	348	93	33.5	820
LMB	This study	CAM3-14	11.99	105.47	2016/10/12	29.3	7.02	204	32	268	91	143	36	16.6	734
LMB	This study	CAM3-18	11.75	105.00	2016/10/14	30.0	6.46	203	34	260	84	139	37	23.6	709
Location	Data source	Sample name	DIC (µmol/L)	Total Alkalinity (µEq/L)	Alkalinity (%)	CAT _{rain}	CAT _{evap+anth}	CAT _{sil} (min)	CAT _{sil} (max)	CAT _{carb} (min)	CAT _{carb} (max)				
<i>Dry season</i>															
Headwater	This study	TLR-04	1169	1168	3.7	22.0	5.5	7.9	66.4	68.7					
UMB	This study	TLR-09	2892	2922	0.9	50.3	8.2	13.1	35.7	40.6					
UMB	This study	TLR-10	2814	2786	1.0	49.1	7.2	11.4	38.5	42.7					
UMB	This study	TLR-11	2732	2751	1.0	48.2	7.4	11.7	39.0	43.3					
UMB	This study	TLR-12	2761	2741	1.0	48.1	6.8	10.7	40.2	44.1					
MMB	This study	TLR-14	1892	1849	1.9	37.3	6.2	9.6	51.3	54.6					
MMB	This study	AR-1	–	–	1.9	36.6	4.0	5.7	55.8	57.5					
LMB	This study	CAMI-11	1628	1641	2.7	29.4	8.8	13.3	54.6	59.2					
LMB	This study	CAMI-8	1596	1589	2.7	29.9	7.7	11.5	55.9	59.7					
LMB	This study	CAMI-9	1570	1600	2.7	29.4	7.4	11.1	56.8	60.5					
<i>Rainy season</i>															
Headwater	*	CJ-218	519	512	7.4	19.9	8.6	13.7	59.0	64.1					
Headwater	*	CJ-223	2226	2199	2.0	21.9	3.8	6.0	70.1	72.3					
Headwater	*	TR-111	1126	1059	5.0	15.4	11.7	18.2	61.4	67.9					
UMB	*	CJ-221	2355	2038	1.8	35.7	10.7	17.1	45.4	51.8					
UMB	*	CJ-217	2294	2175	1.5	38.7	10.3	16.3	43.5	49.5					
UMB	*	TR-118	2472	2444	1.5	39.9	10.0	15.9	42.6	48.6					

Table 1 (continued)

Location	Data source	Sample name	DIC ($\mu\text{mol/L}$)	Total Alka- linity ($\mu\text{Eq/L}$)	CAT _{rain} (%)	CAT _{evap+anth}	CAT _{sil} (min)	CAT _{sil} (max)	CAT _{carb} (min)	CAT _{carb} (max)
UMB	*	TR-112	2157	2111	1.8	31.4	8.7	14.0	52.7	58.0
MMB	*	RD-129	2009	2019	2.1	28.9	10.4	16.5	52.4	58.6
MMB	*	RD-126	1842	1848	2.3	28.4	10.5	16.7	52.6	58.7
LMB	This study	CAM2-12	950	875	4.0	36.7	5.7	7.4	52.0	53.7
LMB	This study	CAM2-14	878	823	4.1	36.3	6.2	8.1	51.5	53.4
LMB	This study	CAM3-14	884	735	6.2	21.6	13.8	21.0	51.3	58.4
LMB	This study	CAM3-18	1231	709	6.4	22.1	15.0	22.7	48.8	56.5

Calculated contributions of silicate weathering, carbonate weathering, evaporite + anthropogenic inputs, and rain to the total cationic charge balance are also shown for each sample

UMB upper Mekong Basin, MMB middle Mekong Basin, LMB lower Mekong Basin

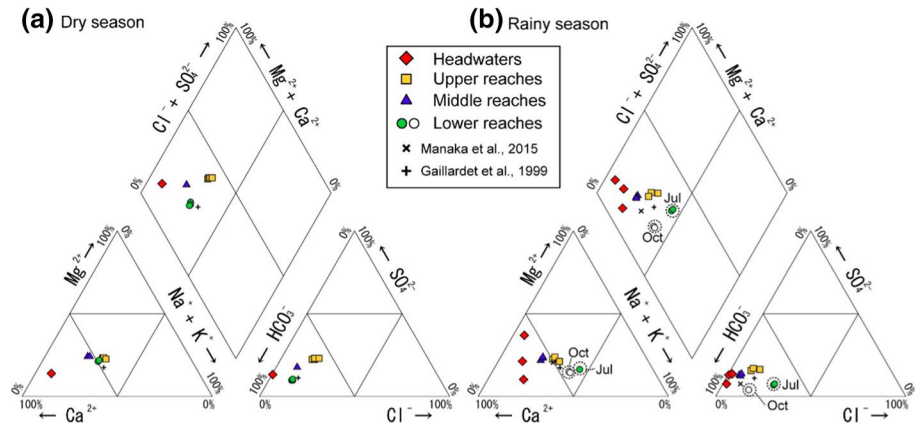


Fig. 3 Trilinear diagram of the major ion composition of river water samples in: **a** the dry season, and **b** the rainy season. Data of Gaillardet et al. (1999) and Manaka et al. (2015b) are also shown

in each basin and season. The major element concentrations of this study did not deviate substantially from those determined by previous studies (Wu et al. 2008a; Manaka et al. 2015b).

Total dissolved cation ($TZ^+ = K^+ + Na^+ + 2Ca^{2+} + 2Mg^{2+}$) concentrations, as a measure of the total dissolved content, were 1597–6381 $\mu\text{Eq/L}$ during the dry season. TZ^+ concentrations were 805–3939 $\mu\text{Eq/L}$ in the rainy season, which were approximately one and a half to two times higher than those in the rainy season. Spatial variations of TZ^+ showed similar trends in both dry and rainy seasons, being relatively low in the headwaters (805–3001 $\mu\text{Eq/L}$), significantly higher in the mainstream of the UMB (1196–6382 $\mu\text{Eq/L}$), then decreasing progressively toward LMB (925–2232 $\mu\text{Eq/L}$) (Fig. S4). Total dissolved anion ($TZ^- = Cl^- + 2SO_4^{2-} + NO_3^- + HCO_3^-$) concentrations fluctuated in a similar way to TZ^+ for all analyzed samples and the normalized inorganic charge balance ($NICB = (TZ^+ - TZ^-)/(TZ^+ + TZ^-)$) ranged from -1 to 3% , which indicated that unanalyzed organic anions were only minor components.

4 Discussion

4.1 Chemical Characteristics of the Mekong River

The ternary diagram of the major ion compositions shows that all analyzed samples were calcium bicarbonate type, similar to the water chemistry characteristics of the Ganges, Brahmaputra, Ayeyarwady, and Yangtze Rivers, which all originate from the Himalayas (Li and Zhang 2005; Manaka et al. 2015a, b; Samanta et al. 2019). The highest TZ^+ and TZ^- concentrations were recorded in the upper reaches and were higher than those in the headwaters of different small basins (Table 1; Fig. S4). This can be attributed to active chemical weathering in the mountainous area where active physical denudation increases the surface area for water–rock interaction (Fig. S2a). On the other hand, TZ^+ and TZ^- continued to decrease from the middle to lower reaches, which may be due to dilution with rainfall which increases as the Mekong River flows downstream. A similar trend can be

seen in the Brahmaputra and Yangtze Rivers, which originate from the eastern Himalayas and flow under the influence of the monsoon (Singh et al. 2005; Wu et al. 2008b).

Considering that the balance of cations and anions is derived predominantly from the chemical weathering of continental rocks, it is unlikely to exhibit major changes unless intermixing occurs between waters from drainage basins with different lithologies. However, the ternary diagram shows that the water quality in the LMB varied significantly between the different seasons, whereas those in the UMB and MMB areas were approximately constant (Fig. 3). Therefore, we suggest that the water source in the LMB changes between dry and rainy seasons but is almost constant in the UMB and MMB.

4.2 Sources of Dissolved Load

4.2.1 Calculation Model

To reveal the spatial and seasonal characteristics of chemical weathering in the Mekong Basin, we calculated the contribution of silicate weathering to the total cationic charge balance in the river waters, i.e., the total alkalinity budget. There are many ways to estimate the relative contributions of the different sources (e.g., Bickle et al. 2018); however, we used the forward modeling approach suggested by Galy and France-Lanord (1999), which has been used in previous studies on the Mekong River (Noh et al. 2009; Li et al. 2014; Manaka et al. 2015b) and other rivers referred to in this paper (West et al. 2005; Moon et al. 2007; Xu and Liu 2007, 2010; Chetelat et al. 2008; Li et al. 2009; Han et al. 2010; Wen et al. 2010; Wang et al. 2016; Bastia and Equeenuddin 2019). In this study, the model outline and calculation conditions followed those of Noh et al. (2009), which considers reservoirs, rain (atmospheric), evaporite, anthropogenic input, silicate, and carbonate. The budget equation for any soluble element X in the river can be written as

$$[X]_{\text{riv}} = [X]_{\text{rain}} + [X]_{\text{evap}} + [X]_{\text{anth}} + [X]_{\text{sil}} + [X]_{\text{carb}}, \quad (1)$$

where $[X]$ represents the molar concentration of X. Subscript notations indicate the origin of the elements; “riv” and “rain” indicate river and rain waters; “evap” and “anth” indicate the input from evaporite dissolution and anthropogenic origins; and “sil” and “carb” represent the contribution from silicate and carbonate weathering, respectively.

It was necessary to correct for the inputs from rain in order to distinguish the lithological origins of the dissolved load. Cl concentrations are very low in all rocks except evaporite, which is the most useful reference for evaluating rain inputs to rivers (e.g., Négrel et al. 1993; Roy et al. 1999). However, we did not analyze rainwater chemistry in the Mekong Basin, and the lowest Cl concentration in the headwater (TLR-04, 3.6 $\mu\text{mol/L}$) was assumed to have been supplied entirely by rain, imitating the assumption of Noh et al. (2009). We calculated the concentrations of other major ions in rain using the elemental ratios in precipitation for Lhasa, Tibet ($[\text{Cl}]_{\text{rain}}/[\text{Na}]_{\text{rain}} = 2.35$, $[\text{SO}_4]_{\text{rain}}/[\text{Na}]_{\text{rain}} = 1.78$, $[\text{K}]_{\text{rain}}/[\text{Na}]_{\text{rain}} = 2.13$, $[\text{Ca}]_{\text{rain}}/[\text{Na}]_{\text{rain}} = 17.04$, $[\text{Mg}]_{\text{rain}}/[\text{Na}]_{\text{rain}} = 0.65$) (Zhang et al. 2003). These ratios are similar in order throughout the entire basin (Li et al. 2014 and references therein).

Following the rain correction, we estimated the contributions from evaporites and anthropogenic inputs. Cl, SO_4 , and Na often have suspected anthropogenic origins from sources such as agricultural fertilizers, animal waste, and municipal and industrial effluents (Li et al. 2009, 2014; Han et al. 2010). However, their contributions to K, Ca, and Mg were negligible because their anthropogenic sources are minor. We assumed that all Cl in river

water remaining after the rain correction originated from halite and anthropogenic inputs, and that all SO_4 originated from gypsum/anhydrite and anthropogenic inputs. As it is difficult to accurately distinguish between halite and anthropogenic sources, both were evaluated together in this study.

$$[\text{Na}]_{\text{evap}} + [\text{Na}]_{\text{anth}} = [\text{Cl}]_{\text{evap}} + [\text{Cl}]_{\text{anth}} = [\text{Cl}]_{\text{river}} - [\text{Cl}]_{\text{rain}} \quad (2)$$

$$[\text{Ca}]_{\text{evap}} + [\text{Mg}]_{\text{evap}} = [\text{SO}_4]_{\text{evap}} + [\text{SO}_4]_{\text{anth}} = [\text{SO}_4]_{\text{riv}} - [\text{SO}_4]_{\text{rain}} \quad (3)$$

The majority of Na remaining after rain, halite, and anthropogenic input corrections, as well as the majority of remaining K after the rain correction, are derived from silicate weathering (Wu et al. 2008a). Ca_{sil} and Mg_{sil} are obtained from Na_{sil} using appropriate $(\text{Ca}/\text{Na})_{\text{sil}}$ and $(\text{Mg}/\text{Na})_{\text{sil}}$ ratios. For the broad Mekong Basin, we do not have a comprehensive dataset of the wide variety of local bedrock, which ranges from mafic to felsic volcanic and plutonic rocks. Therefore, we assumed a wide range of values, i.e., $(\text{Ca}/\text{Na})_{\text{sil}} = 0.35 \pm 0.15$ (mol/mol), $(\text{Mg}/\text{Na})_{\text{sil}} = 0.24 \pm 0.12$ (mol/mol), which were based on different river basins all over the world (Gaillardet et al. 1999). This range covers the assumed values used in previous studies for Himalayan river basins including the Yangtze (Chetelat et al. 2008), Red (Moon et al. 2007), and Ganges–Brahmaputra Rivers (Galy and France-lanord 1999).

$$[\text{Na}]_{\text{sil}} = [\text{Na}]_{\text{riv}} - [\text{Na}]_{\text{rain}} - [\text{Na}]_{\text{evap}} - [\text{Na}]_{\text{anth}} \quad (4)$$

$$[\text{K}]_{\text{sil}} = [\text{K}]_{\text{riv}} - [\text{K}]_{\text{rain}} \quad (5)$$

$$[\text{Ca}]_{\text{sil}} = [\text{Na}]_{\text{sil}} \times (\text{Ca}/\text{Na})_{\text{sil}} \quad (6)$$

$$[\text{Mg}]_{\text{sil}} = [\text{Na}]_{\text{sil}} \times (\text{Mg}/\text{Na})_{\text{sil}} \quad (7)$$

Given these ratios, the cationic charge contributions (%) derived from rain (CAT_{rain}), evaporite + anthropogenic inputs ($\text{CAT}_{\text{evap+anth}}$), silicate (CAT_{sil}), and carbonate (CAT_{carb}) to the cationic charge balance (total alkalinity budgets) can be calculated as follows, where the sample analysis results are listed in Table 1:

$$\text{CAT}_{\text{rain}} = 100 \times ([\text{Na}]_{\text{rain}} + [\text{K}]_{\text{rain}} + 2 \times [\text{Ca}]_{\text{rain}} + 2 \times [\text{Mg}]_{\text{rain}}) / ([\text{Na}]_{\text{riv}} + [\text{K}]_{\text{riv}} + 2 \times [\text{Ca}]_{\text{riv}} + 2 \times [\text{Mg}]_{\text{riv}}) \quad (8)$$

$$\text{CAT}_{\text{evap+anth}} = 100 \times ([\text{Na}]_{\text{evap}} + [\text{Na}]_{\text{anth}} + 2 \times [\text{Ca}]_{\text{evap}} + 2 \times [\text{Mg}]_{\text{evap}}) / ([\text{Na}]_{\text{riv}} + [\text{K}]_{\text{riv}} + 2 \times [\text{Ca}]_{\text{riv}} + 2 \times [\text{Mg}]_{\text{riv}}) \quad (9)$$

$$\text{CAT}_{\text{sil}} = 100 \times ([\text{Na}]_{\text{sil}} + [\text{K}]_{\text{sil}} + 2 \times [\text{Ca}]_{\text{sil}} + 2 \times [\text{Mg}]_{\text{sil}}) / ([\text{Na}]_{\text{riv}} + [\text{K}]_{\text{riv}} + 2 \times [\text{Ca}]_{\text{riv}} + 2 \times [\text{Mg}]_{\text{riv}}) \quad (10)$$

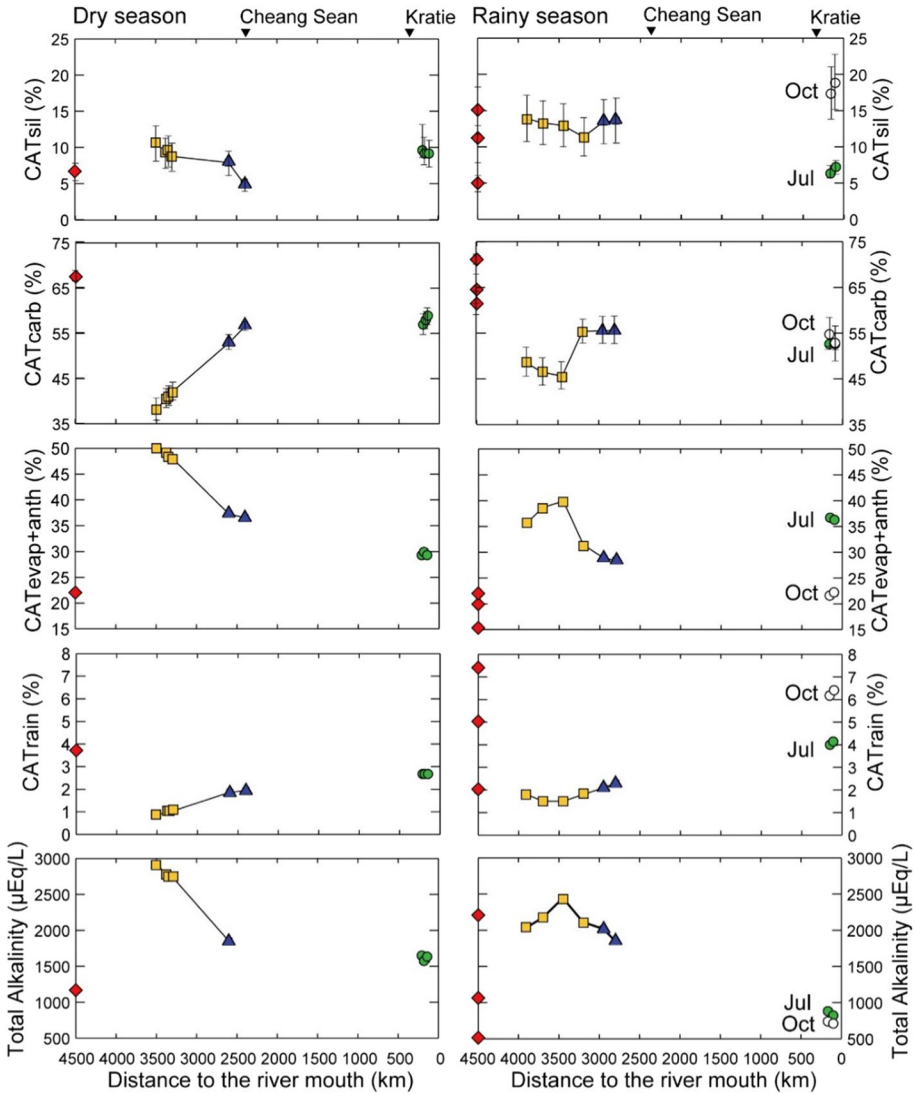


Fig. 4 Total contributions of silicate weathering, carbonate weathering, evaporite dissolution anthropogenic inputs, and rain to the total cationic charge balance for each sample, as well as total alkalinity values. The values of several headwater samples from different small tributaries in the upper Mekong Basin (UMB) are plotted at the left of each graph. The legend for each point is the same as that in Fig. 3. Open circles represent data from the flooding season (October) in the LMB. The left and right columns represent dry and rainy seasons, respectively

$$\begin{aligned}
 \text{CAT}_{\text{carb}} = 100 \times \left\{ 2 \times ([\text{Ca}]_{\text{riv}} - [\text{Ca}]_{\text{rain}} - [\text{Ca}]_{\text{evap}} - [\text{Ca}]_{\text{sil}}) \right. \\
 \left. + 2 \times ([\text{Mg}]_{\text{riv}} - [\text{Mg}]_{\text{rain}} - [\text{Mg}]_{\text{evap}} - [\text{Mg}]_{\text{sil}}) \right\} / \quad (11) \\
 ([\text{Na}]_{\text{riv}} + [\text{K}]_{\text{riv}} + 2 \times [\text{Ca}]_{\text{riv}} + 2 \times [\text{Mg}]_{\text{riv}})
 \end{aligned}$$

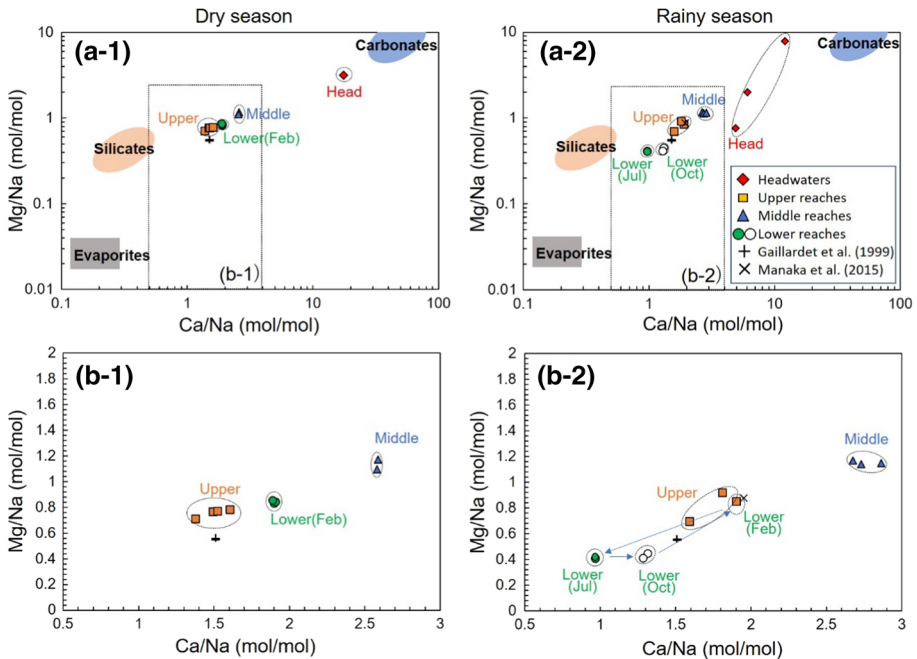


Fig. 5 Variations of Na-normalized Mg relative to Na-normalized Ca on: **a** logarithmic, and **b** linear scales. Dry and rainy season data are shown on the left (**a-1** and **b-1**) and right (**a-2** and **b-2**), respectively. Data from the dry season are also shown in (**b-2**) to illustrate the seasonal changes of these ratios in the lower Mekong Basin (indicated by arrows). End-member reservoirs (silicate, carbonate, and evaporite) were estimated by Gaillardet et al. (1999)

4.2.2 Spatial and Seasonal Variations

The cationic charge contributions (CATs) in the mainstream of the Mekong River exhibited spatial and seasonal fluctuations (Fig. 4). To visualize these characteristics and the controlling factors, we plotted Na-normalized Mg concentrations relative to Na-normalized Ca concentrations (Fig. 5). As first pointed out by Gaillardet et al. (1999), this plot illustrates mixing among silicate, carbonate, and evaporite weathering. The end members were estimated using data from small rivers draining a single lithology. It is evident that large seasonal variations in the source of the dissolved load in the LMB, whereas the source is almost constant in the MMB and UMB.

The CAT_{carb} values were 35.7–72.3%, which were remarkably higher than the CAT_{sil} values of 3.8–22.7% (Table 1), which is consistent with previous research (Wu et al. 2008a; Li et al. 2014). Our results suggest that the Mekong River is dominated by carbonate weathering. The CAT_{sil} values were relatively high in the UMB and decreased as it flowed in the MMB before increasing again in the LMB, except for during the flooding season. The CAT_{carb} values were low in the UMB and higher in the MMB. These trends in the relative ratios of CAT_{sil} and CAT_{carb} are approximately consistent with the predominant geological features associated with each basin (see Sect. 2.1 and Fig. S3). In the UMB, volcanic rocks and plutonic felsic rocks intruding in the Three Rivers area promote silicate weathering. The MMB mainly consists of carbonate consolidated rocks and limestones,

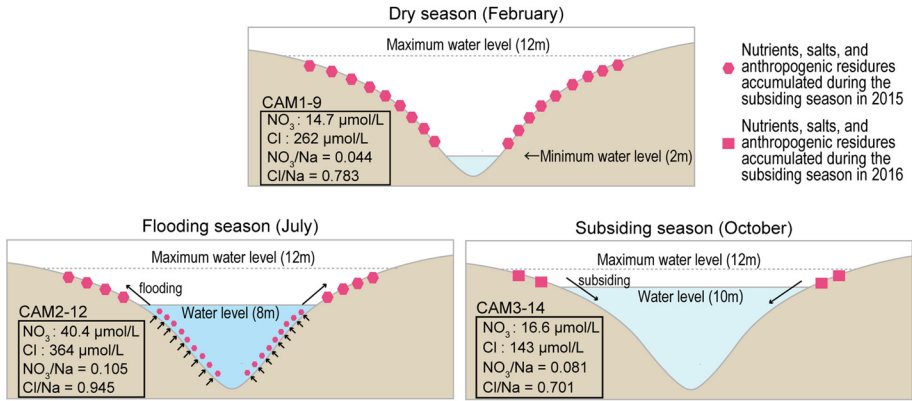


Fig. 6 Schematics of the seasonal variations in the water environment in the lower Mekong Basin in 2016. NO_3^- and Cl^- concentrations, and Cl^-/Na^+ ratios (mol/mol) in each season at the same location (CAM1-9, CAM2-12, and CAM3-14) are shown in the lower left of the figures

which enhance carbonate weathering. In the LMB, relatively siliceous sandstone and mudstone prevail, which may increase CAT_{sil} , except for during the flooding season. The significant decrease in CAT_{sil} values in the flooding season is balanced by an increase in $\text{CAT}_{\text{evap+anth}}$ (Figs. 4, 5), which seems to be controlled by seasonal water level fluctuations in the LMB, as discussed below.

The $\text{CAT}_{\text{evap+anth}}$ values were 15.4–50.3%. They were relatively high in the UMB, lower downstream, and lowest in the LMB, except for during the flooding season. High values in the UMB can be attributed to significantly high evaporation in the source areas in the eastern Tibetan Plateau (e.g., Zhang et al. 2009; Ma et al. 2016). High evaporite contributions (45–83%) to the total dissolved loads were also reported in the upper reaches of the Yangtze and Yellow Rivers, which originate from the Tibetan Plateau (Li and Zhang 2005; Wu et al. 2008b). In the MMB, $\text{CAT}_{\text{evap+anth}}$ values decreased due to dilution.

Large seasonal variations of $\text{CAT}_{\text{evap+anth}}$ in the LMB may be attributed to considerable changes in the river water level and subsequent flooding. Remarkably higher (i.e., almost doubled) Na, Cl, and NO_3^- concentrations were recorded in the flooding season than in the dry season. This could be attributed to the large water discharge and high river water level during the rainy season, which causes heavy flooding every year in Cambodia (MRC, 2005). Floods provide abundant nutrients to surface soils in the hinterland, which support high biological production. A wide range of the hinterland in the LMB is used as rainfed cropland (Pokhrel et al. 2018). Solar salt production also becomes popular during the dry season in northeastern Thailand, Khorat Plateau, where large salt-bearing sedimentary rocks and halite are distributed (El Tabakh et al. 1999). In the flooding season, the expanded river dissolves the nutrient salts originating from the residues of the previous year’s flood, as well as domestic waste, compost, and solar salts deposited during the dry season. Extremely high Cl^- concentrations in the tributaries (i.e., Chi and Mun Rivers) flowing through Khorat Plateau were observed in July (Manaka et al. 2015b), which can affect the water characteristics in the main current of the river. High NO_3^- concentrations in the main current during the flooding season (June–July) were often observed in the lower reaches of the Mekong River (Iida et al. 2007; Oeurng et al. 2016). In 2016, when we sampled water in Cambodia, a maximum water level of 12 m was recorded in August, which

is approximately five to six times higher than that in the dry season (January–May) (MRC, 2016). Our results showed that the increase in NO_3 and Cl concentrations coincide with the increased water level around June (Table 1). Chemical ratios of Cl/Na and NO_3/Na reflect the relative sources of these elements, including salts and agricultural chemicals (Roy et al. 1999). A higher Cl/Na and NO_3/Na ratio in the flooding season than in the other seasons suggests that high Cl and NO_3 contents are not only due to the dissolution of evaporating residue but also from anthropogenic activities such as fertilizers, communal effluents, and industrial sewage (Fig. 6). After these remains are dissolved in the expanded Mekong River, $\text{CAT}_{\text{evap+anth}}$ values become low in the subsiding season. The floodwater leaves a large amount of residue in the hinterland during the subsequent rapid decrease in the river water level, which remains in place until the next flooding season (Fig. 6). This interpretation is also seen in the seasonal cycle of water properties in the mixing model (Fig. 5). Our results suggest that local hydrological phenomena induced by annual flooding and subsiding can also affect the CATs balance in the Mekong River. Therefore, we should carefully consider such effects when we assume the total amount of silicate and carbonate weathering in the entire basin based on water chemical compositions observed in the lower reaches.

The CAT_{rain} values were relatively small (0.9–7.4%) in all sampling sites, especially in the dry season. Relatively high values were recorded in the headwaters and lower reaches, which represented the shorter reaction time with rocks and high precipitation in the LMB, respectively. We can also see that CAT_{rain} increased as rainfall in the LMB increased from February (the dry season) to July (the flooding season) and October (the subsiding season) (Fig. 4).

4.3 CO_2 Consumption Rates

In the above discussion, we revealed the spatial and seasonal variations in the sources of dissolved loads in Mekong River water. Therefore, for an accurate estimate of CO_2 consumption in the river basins using the chemical data of the river water, these changes should be carefully included in the calculation. Total CO_2 consumption in each sub-basin and season was determined using the following cation concentration methodology introduced by previous studies (Wu et al. 2008a; Noh et al. 2009; Manaka et al. 2015b). Cations derived from silicate and carbonate weathering lead to the following equations for calculating CO_2 consumption due to weathering.

$$\Phi\text{CO}_{2\text{evap+anth}} = 0 \quad (12)$$

$$\Phi\text{CO}_{2\text{sil}} = ([\text{Na}]_{\text{sil}} + [\text{K}]_{\text{sil}} + 2 \times [\text{Ca}]_{\text{sil}} + 2 \times [\text{Mg}]_{\text{sil}}) \times \text{total runoff (km}^3) \quad (13)$$

$$\text{CO}_{2\text{sil}} = ([\text{Na}]_{\text{sil}} + [\text{K}]_{\text{sil}} + 2 \times [\text{Ca}]_{\text{sil}} + 2 \times [\text{Mg}]_{\text{sil}}) \times \text{discharge (km}^3/\text{a)} / \text{drainage area (km}^2) \quad (14)$$

$$\Phi\text{CO}_{2\text{carb}} = ([\text{Ca}]_{\text{carb}} + [\text{Mg}]_{\text{carb}}) \times \text{total runoff (km}^3) \quad (15)$$

$$\text{CO}_{2\text{carb}} = ([\text{Ca}]_{\text{carb}} + [\text{Mg}]_{\text{carb}}) \times \text{discharge (km}^3/\text{a)} / \text{drainage area (km}^2) \quad (16)$$

According to these equations, the chemical weathering in the LMB ($\Phi\text{CO}_{2, \text{LMB}}$) can be expressed as:

$$\Phi\text{CO}_{2, \text{LMB}} = \Phi\text{CO}_{2, \text{out, Total basin}} - \Phi\text{CO}_{2, \text{in, UMB\&MMB}} \quad (17)$$

where ΦCO_2 and ϕCO_2 denote total CO_2 consumption (mol) and rate per drainage area ($\text{mol}/\text{km}^2 \text{ a}$), and “out” and “in” represent the river outlet and inlet of the sub-basin, respectively.

Monthly river discharge data are available from the monitoring stations in Chiang Sean and Kratie operated by the MRC, which are located at the boundary of the UMB and MMB and in the lower reaches of the LMB, respectively (Figs. 1, 2). Therefore, we separately calculated CO_2 consumption in the dry and rainy seasons for the UMB & MMB (above Chiang Sean monitoring station), and for the LMB (from Kratie monitoring station to Chiang Sean monitoring station), respectively. The monthly average flow rate from 2000 to 2016, which covers all sampling surveys in this study, was used for the calculation. This separation also reflects the differences of topography and climate in the Mekong Basin, e.g., mountainous and arid in the UMB & MMB and relatively flat and wet in the LMB (Figs. 1, S1). In the dry season, the mean chemical composition data of TLR-14 and AR-1 were used for the calculation in the UMB and MMB, whereas the mean data of CAM1-8, CAM1-9, and CAM1-11 were used for calculations in the LMB. For the rainy season, the mean data of RD-126 and RD-129 were most representative of the UMB and MMB because they are close to the Chiang Sean monitoring station. For the LMB, we used the mean of CAM2-12 and CAM2-14 for the flooding season, and the mean of CAM3-14 and CAM3-18 for the subsiding season. The calculation results are shown in Table 2.

The $\Phi\text{CO}_{2\text{sil}}$ and $\Phi\text{CO}_{2\text{carb}}$ values in the rainy season were three to five times larger than those in the dry season both in the UMB & MMB and LMB (Fig. 7). The chemical weathering rates are governed by multiple parameters including fresh mineral supply rates and climate factors (Riebe et al. 2004; West et al. 2005). The warm and humid climate conditions as well as the abundant mineral supplies with increasing river flow during the rainy season promote chemical weathering (Brady and Carroll 1994; White and Blum 1995; Dalai et al. 2002; West et al. 2005; Li et al. 2016). Enhanced chemical weathering rates during the rainy season have also been suggested for the other river basins in monsoon Asia (e.g., Bastia and Equeenuddin 2019).

The $\Phi\text{CO}_{2\text{sil}}$ and $\Phi\text{CO}_{2\text{carb}}$ values in the UMB & MMB were almost comparable to those in the LMB, even though the area and water discharge of the UMB & MMB were only one-third and one-fifth of those in the LMB, respectively (Table 2). Both $\phi\text{CO}_{2\text{sil}}$ and $\phi\text{CO}_{2\text{carb}}$ values in the UMB & MMB were approximately double those in the LMB although the climate in the lower basin is warmer and damper than that in the upper basin (Fig. 7). This suggests that the amount of mineral supply limits chemical weathering rather than climate factors. Despite the water discharge differing by five times, the amount of suspended sediment generated in the UMB & MMB (195 km^2) is approximately $70\text{--}80 \times 10^9 \text{ kg/a}$, which is almost comparable to that of the LMB (600 km^2) at $80\text{--}90 \times 10^9 \text{ kg/a}$ (Liu et al. 2013). Active physical denudation in the mountainous areas increases the surface area for water–rock interaction and enhances the chemical weathering rate (Millot et al. 2002; Riebe et al. 2004; Singh et al. 2005; Wu et al. 2008b). Relatively high chemical weathering rates in the upper basins have also been observed in the other Himalayan rivers, such as the Yellow and Brahmaputra Rivers (Wang et al. 2016; Samanta et al. 2019). Large temperature differences between day and night, combined with freezing and thawing processes in the Himalayas may lead to a higher physical erosion rate (Huh

Table 2 Calculated total CO₂ consumption and net CO₂ consumption rates of each basin and season in the Mekong River

	Catchment area (10 ³ km ²)	Total runoff (km ³)	CO ₂ consumption (10 ⁹ mol)		Net CO ₂ consumption rate (10 ³ mol / km ² a)					
			ΦCO _{2H} (min)	ΦCO _{2H} (max)	ΦCO _{2carb} (min)	ΦCO _{2carb} (max)	øCO _{2sil} (min)	øCO _{2carb} (min)	øCO _{2carb} (max)	
<i>Dry season (Dec–May)</i>										
Upper-Middle basin	195	21.0	3	5	18	18	35	52	180	188
Lower basin	600	37.9	7	11	19	21	24	35	63	69
Whole basin	795	58.9	10	16	37	39	26	39	92	98
<i>Rainy season (Jun–Nov)</i>										
Upper-Middle basin	195	58.7	17	26	43	48	171	271	446	496
Lower basin	600	276.9	21	28	68	71	70	92	227	238
Whole basin	795	335.6	38	54	111	120	95	136	280	301
<i>Annual (Jan–Dec)</i>										
Upper-Middle basin	195	79.7	20	32	61	67	103	162	313	342
Lower basin	600	394.5	28	38	87	92	47	64	145	154
Whole basin	795	474.3	48	70	148	159	61	88	186	200
Annual (previous studies)										
Gaillardet et al. (1999)	795	467	194		409		244		514	
Li et al. (2014)	795	470	152		228		191		286	
Manaka et al. (2015a, b)	795	467	132	192	389	438	166	241	489	551

Results of previous studies are shown in the bottom three rows

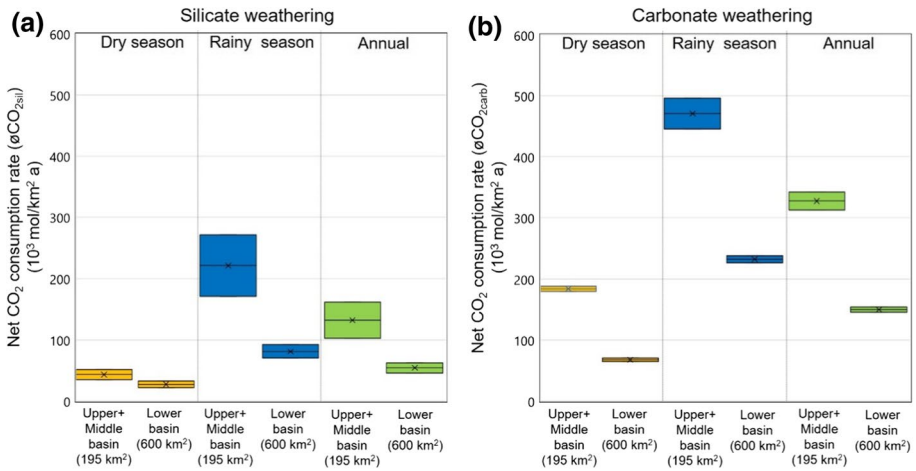


Fig. 7 Net CO₂ uptake rates by: **a** silicate weathering, and **b** carbonate weathering

and Edmond 1999). In addition, due to the high elevation of ice-covered mountains with deep valleys, water from ice and snow melting may travel long distances and be subjected to several leaching and oozing processes before flowing into the river, and the relationships between recharge and discharge of groundwater and surface waters can be reversed, resulting in intense water–rock interactions (Cheng and Jin 2013). Our results suggest that a higher physical denudation rate in the upper basins leads to a significant increase in the chemical weathering rate.

Summing up the CO₂ consumption for the entire Mekong Basin is 48–70 × 10⁹ mol/a and 148–159 × 10⁹ mol/a due to silicate and carbonate weathering, respectively. These values were less than half the previous estimates by Gaillardet et al. (1999), according to a similar calculation model (Table 2). These discrepancies cannot be attributed to differences in the climate between previous studies and our survey years because changes in annual temperature and precipitation in the previous 50 years have been limited to within 5% (Pokhrel et al. 2018). Moreover, the reduction of water discharge due to dam construction in the 1990s is less than 10% (Pokhrel et al. 2018), which also cannot account for these differences. Our results are also smaller than those assumed by Li et al. (2014), using different mass balance calculations and estimating the contributions of evaporite dissolution and anthropogenic inputs to certain small values (Table 2). However, as discussed in Sect. 4.2, these contributions may fluctuate seasonally by as much as one-third of the total cationic charge balance in the flooding season; therefore, we disagree with their assumption.

Thus, we propose that multiple inter-basin and inter-season calculations that consider various reactions that supply elements to river water are necessary for the accurate estimation of chemical weathering fluxes in the Mekong Basin. This approach should also be applied to other Himalayan rivers because of the large seasonal and spatial variations in weathering reactions in the lower reaches. Therefore, the total amount of CO₂ consumption in the Himalayas as assessed by Gaillardet et al. (1999) should be carefully reviewed to correctly evaluate the contribution of chemical weathering to global climate change.

5 Conclusions

To understand the spatial and seasonal variations of chemical weathering in the Mekong Basin, we separately estimated the source of dissolved ions and calculated the net CO₂ consumption rates from the upper to lower basin, in the dry and rainy seasons using multiple water chemistry data. The following major conclusions were drawn:

1. Changes in the assumed relative contributions of rain, anthropogenic inputs, evaporite dissolution, and silicate and carbonate weathering to the cationic charge balance of river water reflect the geological and climate variations from the upper to lower basins. In the lower reaches, large seasonal water level fluctuations and related floods also influence water quality.
2. The chemical weathering rates in the rainy season were three to five times higher than those in the dry season, which may be attributed to high temperature and precipitation.
3. In the middle to upper basin, strong physical denudation enhanced the chemical weathering rate, resulting in approximately twice the CO₂ consumption as high as that in the lower basin.
4. The total CO₂ consumption in the Mekong Basin was almost half that of previous estimates, which suggests that numerous sampling efforts, covering entire basins and seasons, are important for ensuring accurate assessments of chemical weathering in large Himalayan river basins.

Acknowledgements We would like to thank students and researchers at Yunnan University for their great help in the fieldwork. We also thank for valuable suggestions that helped to improve this manuscript by Editor Dr. Marc Benedetti and anonymous reviewers. This research was partly supported by the Graduate Research Abroad in Science Program (GRASP) of the University of Tokyo for H. Kajita. It was also jointly supported by the Second Tibetan Plateau Scientific Expedition and Research (STEP) (2019QZKK0704), the Strategic Priority Research Program of Chinese Academy of Sciences (XDB26020301), and National Natural Science Foundation of China (NSFC) (U1902208, 41991323) to H. Zheng.

Author's Contributions HK and HK contributed to the study conception and design. Sample collection in the upper reaches was performed by HK and ZO. Sample collection in the middle and lower reaches was performed by HK, HK, YO, DA, SI, TY, and AS. On-site management during fieldwork was performed by KW, QY, HZ, and EU. Laboratory analyses were conducted by HK, YO, TY, and AI. The first draft of the manuscript was written by HK. All authors read and approved the final manuscript.

Compliance with Ethical Standards

Conflict of interest The authors declare that they have no conflict of interest.

References

- Amiotte Suchet P, Probst J-L, Ludwig W (2003) Worldwide distribution of continental rock lithology: implications for the atmospheric/soil CO₂ uptake by continental weathering and alkalinity river transport to the oceans. *Global Biogeochem Cycles* 17(2):1038. <https://doi.org/10.1029/2002gb001891>
- Bastia F, Equeenuddin S (2019) Chemical weathering and associated CO₂ consumption in the Mahanadi river basin, India. *J Asian Earth Sci* 174:218–231. <https://doi.org/10.1016/j.jseas.2018.12.010>
- Berner RA (2003) The long-term carbon cycle, fossil fuels and atmospheric composition. *Nature* 426:323–326. <https://doi.org/10.1038/nature02131>

- Berner RA, Lasaga AC, Garrels RM (1983) The carbonate-silicate geochemical cycle and its effect on atmospheric carbon dioxide over the past 100 million years. *Am J Sci* 283:641–683
- Bickle MJ, Chapman HJ, Tipper E et al (2018) Chemical weathering outputs from the flood plain of the Ganga. *Geochim Cosmochim Acta* 225:146–175. <https://doi.org/10.1016/j.gca.2018.01.003>
- Brady PV, Carroll SA (1994) Direct effects of CO₂ and temperature on silicate weathering: possible implications for climate control. *Geochim Cosmochim Acta* 58:1853–1856
- Cheng G, Jin H (2013) Permafrost and groundwater on the Qinghai-Tibet plateau and in northeast China. *Hydrogeol J* 21:5–23. <https://doi.org/10.1007/s10040-012-0927-2>
- Chetelat B, Liu CQ, Zhao ZQ et al (2008) Geochemistry of the dissolved load of the Changjiang Basin rivers: Anthropogenic impacts and chemical weathering. *Geochim Cosmochim Acta* 72:4254–4277. <https://doi.org/10.1016/j.gca.2008.06.013>
- Dalai TK, Krishnaswami S, Sarin MM (2002) Major ion chemistry in the headwaters of the Yamuna river system. *Geochim Cosmochim Acta* 66:3397–3416. [https://doi.org/10.1016/S0016-7037\(02\)00937-7](https://doi.org/10.1016/S0016-7037(02)00937-7)
- El Tabakh M, Utha-Aroon C, Schreiber BC (1999) Sedimentology of the cretaceous Maha Sarakham evaporites in the Khorat Plateau of northeastern Thailand. *Sediment Geol* 123:31–62. [https://doi.org/10.1016/S0037-0738\(98\)00083-9](https://doi.org/10.1016/S0037-0738(98)00083-9)
- Feng QL (2002) Stratigraphy of volcanic rocks in the Changning-Menglian Belt in southwestern Yunnan, China. *J Asian Earth Sci* 20:657–664. [https://doi.org/10.1016/S1367-9120\(02\)00006-8](https://doi.org/10.1016/S1367-9120(02)00006-8)
- Gaillardet J, Dupre B, Louvat P, Allegre CJ (1999) Global silicate weathering and CO₂ consumption rates deduced from the chemistry of large rivers. *Chem Geol* 159:3–30. [https://doi.org/10.1016/S0009-2541\(99\)00031-5](https://doi.org/10.1016/S0009-2541(99)00031-5)
- Galy A, France-Ianord C (1999) Weathering processes in the Ganges-Brahmaputra basin and the riverine alkalinity budget. *Chem Geol* 159:31–60
- Gupta A (2009) Geology and landforms of the Mekong Basin. *The Mekong* 3:29–51. <https://doi.org/10.1016/B978-0-12-374026-7.00003-6>
- Han G, Tang Y, Xu Z (2010) Fluvial geochemistry of rivers draining karst terrain in Southwest China. *J Asian Earth Sci* 38:65–75. <https://doi.org/10.1016/j.jseae.2009.12.016>
- Hodges K (2006) Climate and the evolution of mountains. *Sci Am* 295:72–79
- Huh Y, Edmond JM (1999) The fluvial geochemistry of the rivers of Eastern Siberia: III. Tributaries of the Lena naba draining the basement terrain of the Siberian Craton and the Trans-Baikal highlands. *Geochim Cosmochim Acta* 63:967–987. [https://doi.org/10.1016/S0016-7037\(99\)00045-9](https://doi.org/10.1016/S0016-7037(99)00045-9)
- Iida T, Inkhamseng S, Yodhida K, Ito S (2007) Seasonal variation in nitrogen and phosphorus concentrations in the Mekong River at Vientiane. *J Jpn Soc Hydrol Water Resour* 20:226–234. <https://doi.org/10.3178/jjshwr.20.226>
- Li G, Hartmann J, Derry LA et al (2016) Temperature dependence of basalt weathering. *Earth Planet Sci Lett* 443:59–69. <https://doi.org/10.1016/j.epsl.2016.03.015>
- Li J-Y, Zhang J (2005) Chemical weathering process and atmospheric CO₂ consumption of Huanghe river and Changjiang river basins. *Chin Geogr Sci* 15:16–21
- Li S, Lu XX, Bush RT (2014) Chemical weathering and CO₂ consumption in the Lower Mekong River. *Sci Total Environ* 472:162–177. <https://doi.org/10.1016/j.scitotenv.2013.11.027>
- Li S, Xu Z, Wang H et al (2009) Geochemistry of the upper Han River basin, China. 3: anthropogenic inputs and chemical weathering to the dissolved load. *Chem Geol* 264:89–95. <https://doi.org/10.1016/j.chemgeo.2009.02.021>
- Liu C, He Y, Des Walling E, Wang J (2013) Changes in the sediment load of the Lancang-Mekong River over the period 1965–2003. *Sci China Technol Sci* 56:843–852. <https://doi.org/10.1007/s11443-013-5162-0>
- Ma N, Szilagyi J, Niu GY et al (2016) Evaporation variability of Nam Co Lake in the Tibetan Plateau and its role in recent rapid lake expansion. *J Hydrol* 537:27–35. <https://doi.org/10.1016/j.jhydr.2016.03.030>
- Manaka T, Araoka D, Yoshimura T et al (2017) Downstream and seasonal changes of lithium isotope ratios in the Ganges-Brahmaputra river system. *Geochem Geophys Geosyst* 18:3003–3015. <https://doi.org/10.1002/2016GC006738>
- Manaka T, Otani S, Inamura A et al (2015a) Chemical weathering and long-term CO₂ consumption in the Ayeyarwady and Mekong river basins in the Himalayas. *J Geophys Res Biogeosci*. <https://doi.org/10.1002/2015JG002932>
- Manaka T, Ushie H, Araoka D et al (2015b) Spatial and seasonal variation in surface water pCO₂ in the Ganges, Brahmaputra, and Meghna Rivers on the Indian subcontinent. *Aquat Geochem* 21:437–458. <https://doi.org/10.1007/s10498-015-9262-2>
- Mekong River Commission (2005) Overview of the hydrology of the Mekong Basin. Mekong River Commission, Vientiane

- Mekong River Commission (2016) Annual report 2016 version 2.0. Mekong River Commission, Vientiane
- Meybeck M, Ragu A (1997) River discharges to the oceans: an assessment of suspended solids, major ions and nutrients. Laboratoire de Géologie Appliquée, Université Pierre et Marie Curie, Paris
- Meybeck M, Ragu A (2012) GEMS-GLORI world river discharge database. Laboratoire de Géologie Appliquée, Université Pierre et Marie Curie, Paris
- Millero FJ (1979) The thermodynamics of the carbonate system in seawater. *Geochim Cosmochim Acta* 43(11–12):1651–1661. [https://doi.org/10.1016/0016-7037\(79\)90184-4](https://doi.org/10.1016/0016-7037(79)90184-4)
- Millot R, Gaillardet J, Dupré B, Allègre CJ (2002) The global control of silicate weathering rates and the coupling with physical erosion: new insights from rivers of the Canadian Shield. *Earth Planet Sci Lett* 196:83–98. [https://doi.org/10.1016/S0012-821X\(01\)00599-4](https://doi.org/10.1016/S0012-821X(01)00599-4)
- Moon S, Huh Y, Qin J, van Pho N (2007) Chemical weathering in the Hong (Red) River basin: rates of silicate weathering and their controlling factors. *Geochim Cosmochim Acta* 71:1411–1430. <https://doi.org/10.1016/j.gca.2006.12.004>
- Négrel P, Allègre CJ, Dupré B, Lewin E (1993) Erosion sources determined by inversion of major and trace element ratios and strontium isotopic ratios in river: the Congo Basin case. *Earth Planet Sci Lett* 120:59–76. [https://doi.org/10.1016/0012-821X\(93\)90023-3](https://doi.org/10.1016/0012-821X(93)90023-3)
- Noh H, Huh Y, Qin J, Ellis A (2009) Chemical weathering in the three rivers region of Eastern Tibet. *Geochim Cosmochim Acta* 73:1857–1877. <https://doi.org/10.1016/j.gca.2009.01.005>
- Oeurng C, Cochrane TA, Arias ME et al (2016) Assessment of changes in riverine nitrate in the Sesan, Srepok and Sekong tributaries of the Lower Mekong River Basin. *J Hydrol Reg Stud* 8:95–111. <https://doi.org/10.1016/j.ejrh.2016.07.004>
- Pokhrel Y, Burbano M, Roush J et al (2018) A review of the integrated effects of changing climate, land use, and dams on Mekong river hydrology. *Water (Switzerland)* 10:1–25. <https://doi.org/10.3390/w10030266>
- Rai SK, Singh SK (2007) Temporal variation in Sr and $^{87}\text{Sr}/^{86}\text{Sr}$ of the Brahmaputra: implications for annual fluxes and tracking flash floods through chemical and isotope composition. *Geochem Geophys Geosyst* 8:1–14. <https://doi.org/10.1029/2007GC001610>
- Raymo ME, Ruddiman WF (1992) Tectonic forcing of late Cenozoic climate. *Nature* 359:117–122
- Riebe CS, Kirchner JW, Finkel RC (2004) Erosional and climatic effects on long-term chemical weathering rates in granitic landscapes spanning diverse climate regimes. *Earth Planet Sci Lett* 224:547–562. <https://doi.org/10.1016/j.epsl.2004.05.019>
- Robbins LL, Hansen ME, Kleypas JA, Meylan SC (2010) CO₂calc: a user-friendly seawater carbon calculator for Windows, Mac OS X and iOS (iPhone), U.S. Geol Surv. Open File Rep, 2010–1280.
- Roy S, Gaillardet J, Allègre CJ (1999) Geochemistry of dissolved and suspended loads of the Seine river, France: anthropogenic impact, carbonate and silicate weathering. *Geochim Cosmochim Acta* 63:1277–1292. [https://doi.org/10.1016/S0016-7037\(99\)00099-X](https://doi.org/10.1016/S0016-7037(99)00099-X)
- Samanta A, Tripathy GR, Das R (2019) Temporal variations in water chemistry of the (lower) Brahmaputra river: implications to seasonality in mineral weathering. *Geochem Geophys Geosyst* 20:2769–2785. <https://doi.org/10.1029/2018GC008047>
- Singh S, Sarin MM, France-Lanord C (2005) Chemical erosion in the eastern Himalaya: major ion composition of the Brahmaputra and $\delta^{13}\text{C}$ of dissolved inorganic carbon. *Geochim Cosmochim Acta* 69:3573–3588. <https://doi.org/10.1016/j.gca.2005.02.033>
- Singh SK, Rai SK, Krishnaswami S (2008) Sr and Nd isotopes in River sediments from the Ganga basin: sediment provenance and spatial variability in physical erosion. *J Geophys Res* 113:1–18. <https://doi.org/10.1029/2007JF000909>
- Tipper ET, Bickle MJ, Galy A et al (2006) The short term climatic sensitivity of carbonate and silicate weathering fluxes: insight from seasonal variations in river chemistry. *Geochim Cosmochim Acta* 70:2737–2754. <https://doi.org/10.1016/j.gca.2006.03.005>
- Tran TV, Tran DX, Myint SW et al (2019) Examining spatiotemporal salinity dynamics in the Mekong River Delta using Landsat time series imagery and a spatial regression approach. *Sci Total Environ* 687:1087–1097. <https://doi.org/10.1016/j.scitotenv.2019.06.056>
- Wang E, Burchfiel BC (2000) Late Cenozoic to Holocene deformation in southwestern Sichuan and adjacent Yunnan, China, and its role in formation of the southeastern part of the Tibetan Plateau. *Geol Soc Am Bull* 112:413–423. [https://doi.org/10.1130/0016-7606\(2000\)112%3C413:LCTHDI%3E2.0.CO;2](https://doi.org/10.1130/0016-7606(2000)112%3C413:LCTHDI%3E2.0.CO;2)
- Wang L, Zhang L, Cai W et al (2016) Consumption of atmospheric CO₂ via chemical weathering in the Yellow River basin: the Qinghai-Tibet Plateau is the main contributor to the high dissolved inorganic carbon in the Yellow River. *Chem Geol* 430:34–44. <https://doi.org/10.1016/j.chemgeo.2016.03.018>
- Wen R, Xiao J, Chang Z et al (2010) Holocene climate changes in the mid-high-latitude-monsoon margin reflected by the pollen record from Hulun Lake, northeastern Inner Mongolia. *Quat Res* 73:293–303. <https://doi.org/10.1016/j.yqres.2009.10.006>

- West AJ, Galy A, Bickle M (2005) Tectonic and climatic controls on silicate weathering. *Earth Planet Sci Lett* 235:211–228. <https://doi.org/10.1016/j.epsl.2005.03.020>
- White AF, Blum AE (1995) Effects of climate on chemical weathering in watersheds. *Geochim Cosmochim Acta* 59:1729–1747
- Wu W, Xu S, Yang J, Yin H (2008a) Silicate weathering and CO₂ consumption deduced from the seven Chinese rivers originating in the Qinghai-Tibet Plateau. *Chem Geol* 249:307–320. <https://doi.org/10.1016/j.chemgeo.2008.01.025>
- Wu W, Yang J, Xu S, Yin H (2008b) Geochemistry of the headwaters of the Yangtze River, Tongtian He and Jinsha Jiang: silicate weathering and CO₂ consumption. *Appl Geochem* 23:3712–3727. <https://doi.org/10.1016/j.apgeochem.2008.09.005>
- Xiaoqi J, Yizhao W, Guanglian X (2003) Devonian to Triassic Successions of the Changning-Menglian Belt, Western Yunnan, China. *Acta Geol Sin* 77:440–456. <https://doi.org/10.1111/j.1755-6724.2003.tb00125.x>
- Xu Z, Liu CQ (2007) Chemical weathering in the upper reaches of Xijiang River draining the Yunnan-Guizhou Plateau, Southwest China. *Chem Geol* 239:83–95. <https://doi.org/10.1016/j.chemgeo.2006.12.008>
- Xu Z, Liu CQ (2010) Water geochemistry of the Xijiang basin rivers, South China: chemical weathering and CO₂ consumption. *Appl Geochem* 25:1603–1614. <https://doi.org/10.1016/j.apgeochem.2010.08.012>
- Yin A, Harrison TM (2000) Geologic evolution of the Himalayan-Tibetan orogen. *Annu Rev Earth Planet Sci* 28:211–280. <https://doi.org/10.1080/01947641003598252>
- Yu Z, Wu G, Keys L et al (2019) Seasonal variation of chemical weathering and its controlling factors in two alpine catchments, Nam Co basin, central Tibetan Plateau. *J Hydrol* 576:381–395. <https://doi.org/10.1016/j.jhydrol.2019.06.042>
- Zhang DD, Peart M, Jim CY et al (2003) Precipitation chemistry of Lhasa and other remote towns. *Tibet Atmos Environ* 37:231–240. [https://doi.org/10.1016/S1352-2310\(02\)00835-X](https://doi.org/10.1016/S1352-2310(02)00835-X)
- Zhang X, Ren Y, Yin ZY et al (2009) Spatial and temporal variation patterns of reference evapotranspiration across the Qinghai-Tibetan Plateau during 1971–2004. *J Geophys Res Atmos* 114:1–14. <https://doi.org/10.1029/2009JD011753>
- Zhong J, Li S, Tao F et al (2017) Impacts of hydrologic variations on chemical weathering and solute sources in the Min River basin, Himalayan-Tibetan region. *Environ Sci Pollut Res* 24:19126–19137. <https://doi.org/10.1007/s11356-017-9584-2>

Publisher's Note Springer Nature remains neutral with regard to jurisdictional claims in published maps and institutional affiliations.

Affiliations

Hiroto Kajita^{1,2,3,4} · Yuki Ota³ · Toshihiro Yoshimura⁴ · Daisuke Araoka³ · Takuya Manaka⁵ · Ouyang Ziyu² · Shinya Iwasaki⁴ · Takuya Yanase^{1,2} · Akihiko Inamura³ · Etsuo Uchida⁶ · Hongbo Zheng⁷ · Qing Yang⁷ · Ke Wang^{2,7} · Atsushi Suzuki³ · Hodaka Kawahata^{1,2,3}

¹ Atmosphere and Ocean Research Institute, The University of Tokyo, Kashiwa, Japan

² Department of Earth and Planetary Science, Graduate School of Science, The University of Tokyo, Tokyo, Japan

³ National Institute of Advanced Industrial Science and Technology (AIST), Tsukuba, Japan

⁴ Japan Agency for Marine-Earth Science and Technology (JAMSTEC), Yokosuka, Japan

⁵ Department of Forest Soils, Forestry and Forest Products Research Institute, Tsukuba, Japan

⁶ School of Creative Science and Engineering, Waseda University, Tokyo, Japan

⁷ Research Center for Earth System Science, Yunnan University, Kunming, China